Available online at www.sciencedirect.com
SCIENCE DIRECT®

Journal of the European Ceramic Society 24 (2004) 413–419

www.elsevier.com/locate/jeurceramsoc

Characterisation of porous silicon nitride materials produced with starch

Aranzazu Díaz*, Stuart Hampshire

Ceramics Research Unit, BM 035 University of Limerick, Limerick, Ireland

Abstract

Porous silicon nitride is gaining interest for a number of applications including metal–ceramic thermal engineering components, biomaterials and catalyst supports. This paper describes the fabrication of porous silicon nitride ceramic materials using a fugitive additive, corn starch, which allows samples to be produced with different volume fractions of porosity from ~0 to 0.25. The initial composition consisted of 92 wt.% Si_3N_4, 6 wt.% Y_2O_3 and 2 wt.% Al_2O_3. Sintering was carried out at 1800 °C for 2 h under nitrogen. Relative density as a function of the fugitive additive content has been measured. Microstructural analysis reveals a dense matrix of elongated β-Si_3N_4 grains surrounded by intergranular glass phase and containing large pores and cavities. Pore size, geometry and grain size have been measured for certain compositions. Young's modulus and modulus of rupture have been determined as a function of the volume fraction of porosity. The Young's modulus–porosity relationship has been compared with previous work in the literature and it was found that this dependency is close to that for a model for spherical pores in cubic stacking arrangement.

Keywords: Grain size; Mechanical properties; Porosity; Si_3N_4; Sintering

1. Introduction

Traditionally, dense silicon nitride has been used to fabricate cutting tools and for high-temperature structural engine applications.[1,2] Silicon nitride has a high mechanical performance which can be outstanding, even with certain levels of porosity, offering an interesting combination of strength and stiffness. This porous silicon nitride is lighter and also can be machined more easily than dense silicon nitride.[3] More recently porous silicon nitride material has acquired interest, as a substitute for the dense material, in Si_3N_4–metal assembled components as a strategy to reduce thermal mismatch between the ceramic and the metal.[4,5] Their potential as catalysts and biomaterials has also been studied. Mesoporous silicon nitride has been suggested as a good candidate for base-catalysed reactions and potassium-loaded high surface area silicon nitride was found to be an efficient superbase catalyst suitable for alkene isomerisation reactions.[6] In the area of biomaterials, their outstanding mechanical properties, fracture toughness, hardness, friction and wear resistance has pin-pointed Si_3N_4-bioglass composites as interesting candidates for many high-load medical applications.[7] The possibility of being able to control the porosity in terms of volume fraction, size and geometry is crucial in order to target particular properties for the final material.

The current work is concerned with the fabrication of porous silicon nitride ceramic materials using a fugitive additive, corn starch, which allows samples with different levels of porosity to be prepared without modifying sintering additives and/or heat treatment conditions. Processing of porous ceramics by starch consolidation has been used to successfully produce porous alumina sintered components[8] and porous interlayers in ceramic laminates.[9] A series of porous silicon nitride materials with volume fraction porosity ranging from ~0 to 0.25 has been prepared and characterised. Relative density as a function of the fugitive additive has been measured. Cross-sections of the materials have been observed using SEM. Pore size, geometry and grain size have been measured for certain compositions. Young's modulus and modulus of rupture have been determined as a function of the volume fraction of porosity.

* Corresponding author. Present address: Instituto de Ciencia de Materiales de Sevilla, Centro Mixto CSIC-Universidad de Sevilla, Centro de Investigaciones Científicas Isla de la Cartuja, Avda, Americo Vespuccio, s/n, 41092 Sevilla, Spain.
E-mail address: arantxad@yahoo.co.uk (A. Díaz).

0955-2219/03/$ - see front matter © 2003 Elsevier Ltd. All rights reserved.
doi:10.1016/S0955-2219(03)00212-7

2. Experimental procedure

2.1. Materials processing

The starting powder consisted of a mixture of 92 wt.% Si_3N_4 (SN-E10, Ube Industries, Ltd, α:β ratio > 0.955, 1.32 wt.% oxygen, particle size 0.5 μm), and 6 wt.% Y_2O_3 (H.C. Starck, purity = 99.99%) and 2 wt.% Al_2O_3 (Aldrich Chemicals, purity = 99.99%). Powders were mixed together in distilled water using attrition milling with silicon nitride milling media. A dispersant (0.02 wt.%, Duramax D3021) was added to minimise agglomeration. The slurry was milled for 2 h at 1000 rpm. Corn starch (Sigma-Aldrich S-4126, particle size 5–18 μm, mean 15 μm, $\rho = 1.49$ g/cm^3) was added at room temperature in varying volumes from 2.5 to 40% keeping the mixture in constant agitation using a magnetic stirrer. A batch free of starch was also prepared as a reference powder to obtain a dense material without fugitive inclusions. The resultant slurry was then frozen and dried under vacuum in a freeze drier (Edwards-Modulyo 4K). Dry powder was sieved (90 μm) and uniaxially pressed at 50 MPa into pellets of size A ($\phi = 20$ mm, $L = 5$ mm) and B ($\phi = 30$ mm, $L = 2.5$ mm) and then isostatically pressed at 150 MPa (only pellets A). Green densities were calculated from measured dimensions and mass. Values vary from $\rho = 1.64$ g/cm^3 for the reference starch free specimen to $\rho = 1.49$ g/cm^3 for that containing 40 vol.% starch. The pellets containing starch were placed in a furnace and heated to 500 °C in air for 2 h using a heating rate of 5 °C/min to burn out the starch. Finally, pellets were packed in a powder bed of composition 50:50 vol.% Si_3N_4(SN-E10):BN (New Metals & Chemicals, Ltd.) in alumina crucibles and sintering was carried out in a graphite furnace (Thermal Technology GMBH) at 1800 °C for 2 h under 0.1 MPa flowing nitrogen (99.999%).

2.2. Materials characterisation

Density and porosity were measured by the Archimedes displacement technique following ASTM C373-88. The phase composition of the samples was determined by X-ray diffraction (XRD) using powder XRD with CuK_α radiation (model X'Pert, Philips Analytical). To prepare the samples for SEM observations, standard metallographic techniques (Buehler supplies) were employed to provide a flat, mirror polish. The samples were first rough ground using Ultra-Prep™ metal bond diamond grinding disc and 30 μm Metadi® polycrystalline diamond suspension. Final polishing was accomplished using progressively diamond suspensions Metadi® from 15 to 1μm. Etching was required in order to distinguish sections of individual grains. Plasma etching was performed in a RF plasma etcher barrel (PT7100) using CF_4/O_2 (8% O_2) gas and an effect of 60W applied. Samples were previously treated in O_2 for 2 min. The etching time was 12 min in two intervals of 6 min. Specimens were observed in secondary electron imaging using a Jeol 820. Quantitative image analysis was carried out using Omnimet Enterprise from Buehler. Typically, 1500 grains of each material were analysed. The Young's modulus was determined at room temperature on pellets A from measurements of the longitudinal (V_l) and transverse (V_t) ultrasonic wave velocities using ASTM E494-92. V_l and V_t were determined with an accuracy better than 0.1%, using two 10 MHz piezoelectric transducers (Ultran). Biaxial flexure strength testing was carried out according to ASTM F394-78 on pellets B.

3. Results and discussion

3.1. Porosity characterisation

To make the pore-containing materials, slurries were formulated with starch content relative to the total volume of solids between 2.5 and 40 vol.% (0.025 and 0.40 vol./unit in Fig. 1). However, the volume fraction of starch in the powder compact depends on the packing density of the ceramic matrix, ρ_m. Slamovich and Lange[10] showed that the volume fraction of inclusions (pores) in a green body resulting from added starch, V_{st}, could be calculated using the following expression:

$$X_{st} = \frac{V_{st}\rho_m}{1 - V_{st} + V_{st}\rho_m} \quad (1)$$

where ρ_m is the relative packing density of the matrix, in this work 0.493 taken to be equal to that of the reference specimen to which no starch was added. If the pores from the fugitive particles (starch) are large enough, they do not themselves sinter but shrink by the same amount as the surrounding matrix and the volume fraction of large pores, X_{st}, in the body will remain according to Eq. (1). Davis et al.[11] studied the sintering

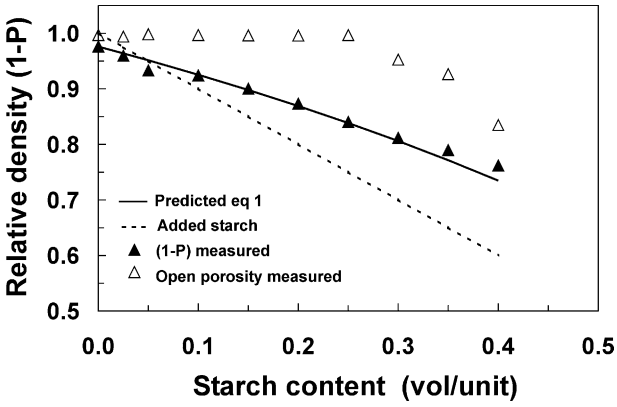

Fig. 1. Relative density ($1-P$) and open porosity versus starch content measured after sintering. Relative density expected from the volume of starch added and values predicted from Eq. (1).[10]

behaviour of alumina with starch and showed sintering was essentially the same as for starch free material suggesting that the added pores from the starch are too large to contribute to the shrinkage. Fig. 1, shows the relative density experimental values, the relative density expected from the volume of starch added to the slurry and the behaviour predicted for Eq. 1. The results show excellent agreement between values predicted from Eq. 1 and the values measured, within the range of porosity studied. Only two compositions with higher porosity level, the ones corresponding to 35 and 40 vol.% starch, appear slightly shifted from the values predicted by expression 1. Open porosity as a function of volume fraction of added starch has also been plotted in Fig. 1. Results indicate measurable open porosity only above 30 vol.% of added starch. Below this level, the pores are closed.

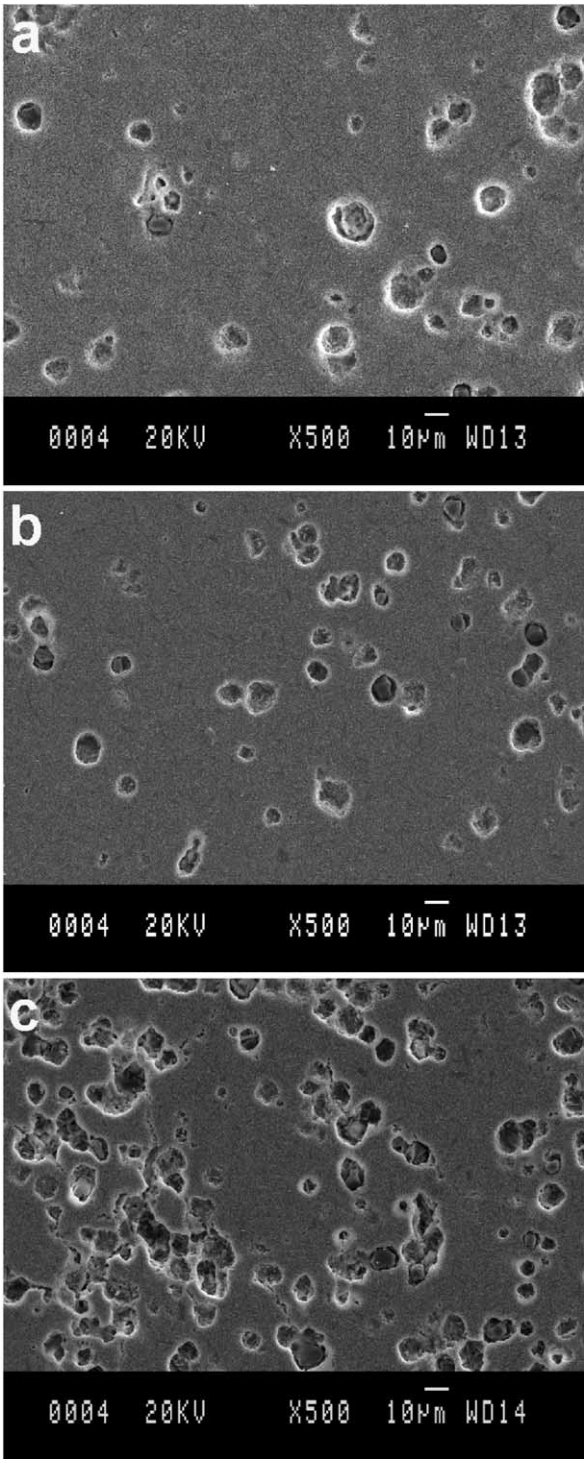

Fig. 2. SEM cross-section micrographs of porous Si_3N_4 materials with (a) 5 vol.% starch, $P=0.07$; (b) 15 vol.% starch, $P=0.10$; (c) 40 vol.% starch, $P=0.24$.

SEM micrographs of cross sections of the porous silicon nitrides prepared with 5, 15 and 40 vol.% starch are shown in Fig. 2. Images show large cavities surrounded by a dense matrix of silicon nitride. The pore size distributions are presented in area percentage in Fig. 3. Values presented here correspond to the equivalent circular diameter of each individual pore in the image. An estimation of the sphericity calculated from the total distribution of pores for the different materials is presented in Table 1, along with the total porosity measured in area fraction. Sphericity has been adopted as a measure of the presence of agglomeration or interconnections between pores. The lower the sphericity the higher the level of interaction of the isolated pores to make bigger cavities or channels. As can be observed in Fig. 2, this level of interconnectivity between pores increases with increasing starch added. This can also be appreciated in analysing the pore size distributions (Fig. 3), which show the presence of bigger cavities with increasing starch content. Higher interconnectivity will open paths and channels between pores, which finally result in open porosity. Results presented in Fig. 1 show that open porosity starts to be measurable for porous materials prepared with more than 30 vol.% of starch which corresponds, approximately to 0.20 volume fraction porosity, P.

3.2. Grain size characterisation

Typical micrographs corresponding to dense regions of the starch-free and the porous materials made using 10 and 20 vol.% of starch are shown in Fig. 4. X-ray diffraction patterns from the materials did not show any α-Si_3N_4 peaks which implies a complete α- to β-Si_3N_4 phase transformation during densification. The β-Si_3N_4

Table 1
Quantitative image analysis of cross section SEM micrographs

Specimen starch volume (%)	Porosity[a] volume fraction (%)	Porosity area fraction (%)	Sphericity (%)
5	6.7	8.4	69
15	10.0	15.6	66
40	23.8	23.8	62

[a] Values obtained previously using the Archimedes displacement technique.

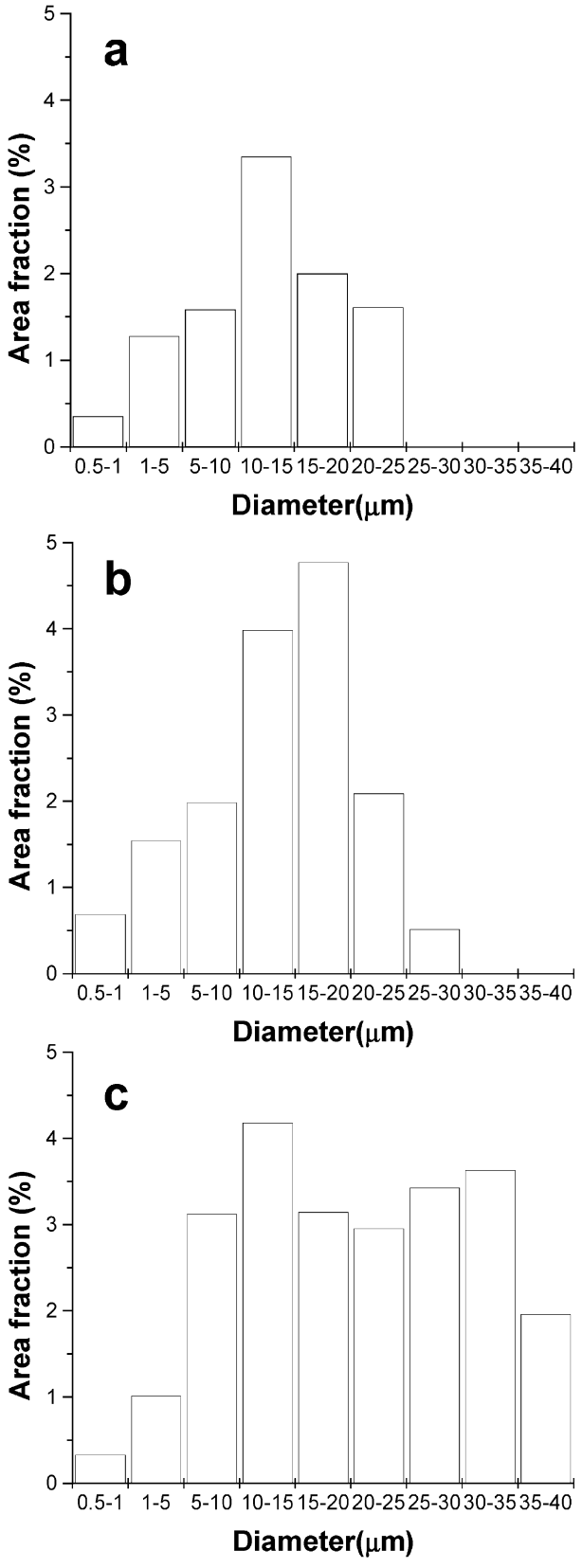

Fig. 3. Pore size distributions obtained using quantitative image analysis of cross-section SEM micrographs of (a) 5 vol.% starch, $P = 0.07$; (b) 15 vol.% starch, $P = 0.10$; (c) 40 vol.% starch, $P = 0.24$.

grains grow as elongated hexagonal prisms. The microstructure of silicon nitride ceramics is characterised by elongated grains embedded in a matrix of finer equiaxed silicon nitride grains and a residual oxynitride grain boundary phase.[12,13] The individual grains are well separated by intergranular films. The lengths and diameters of exposed grains can be determined assuming an elliptical shape. The diameter can be estimated from the shortest diagonal and the length from the longest. However, the determination of the visible length from cross-sections yields random values, depending on the orientation of the section. Based on the assumption that all the β-Si_3N_4 grains in a microstructure have approximately the same aspect ratio, this aspect ratio can be determined as a mean value of the 10% highest apparent aspect ratios on a section, R_{95}.[14,15] In this work, the average diameter, and R_{95} has been measured to characterise grain size of the materials. Table 2 details the microstructural parameters obtained for the materials presented in Fig. 4. The average grain size was 0.26 μm and the mean aspect ratio was 3.7. These microstructural parameters are quite similar in all the materials analysed, which indicates that the introduction of large cavities from the fugitive particles has no effect on final β-Si_3N_4 grain size and the overall microstructure of the sintered matrix material.

3.3. Mechanical properties

Numerous relations have been proposed to relate the elastic moduli and mechanical properties in general to the porosity. Several two-parameter empirical relations have been used to fit modulus-porosity data. A simple linear relation of the form:

$$E = E_o\ (1 - hP) \tag{2}$$

has been found to fit well with a large set of modulus–porosity data over a limited porosity range, especially at lower porosity levels.[16] Interest in predictive tools for porosity-dependent properties has lead to research of a number of models based on the minimum solid area (MSA), micromechanics and microcracks.[17,18] MSA models use geometrical reasoning to predict the elastic moduli based on the weakest points within the structure.

Table 2
Microstructural parameters obtained using quantitative image analysis of polished plasma etched cross-section SEM micrographs

Specimen starch volume (%)	Porosity[a] volume fraction (%)	Mean values		Maximum values	
		Diameter (μm)	Aspect ratio a_{95}	Diameter (μm)	Aspect ratio
0	2.4	0.25	3.80	1.27	6.69
10	7.6	0.29	3.57	1.63	6.86
20	12.7	0.25	3.71	1.41	6.92

[a] Values obtained previously using the Archimedes displacement technique.

It was shown to be approximated by the following exponential relationship:

$$E = E_o \exp(-bP) \quad (3)$$

with different b values depending on pore structure and can be adapted for pore combinations via a weighted average of the b values. Finite-element method (FEM) has also been found useful in cases where the microstructure matched that of the models.[19] However, for real porous materials, studies on the property variations are not normally based on an exhaustive characterisation of the porosity and other interrelated properties. A rigorous porosity characterisation may be a difficult task, particularly for an extended range of porosity if the effects of interaction between adjacent pores, and changes in geometry due to the pore interconnections to form open porosity, have to be addressed. Thus, equations mentioned above may yield inaccurate or unrealistic values over a wide range of porosity. A new equation of the form:

$$E = E_o (1 - aP)^n \quad (4)$$

where a and n are material constants has been found to successfully describe the porosity dependence of Young's modulus over a wide range of porosity in many polycrystalline solids in general[20] and Si_3N_4 in particular.[21]

The experimental values of Young's modulus (E) as a function of porosity measured in this work are plotted in Fig. 5 along with the corresponding regression lines following Eqs. (2)–(4). Experimental points were fitted using the non-linear regression method based on the Levenberg–Marquardt (LM) algorithm. A summary of the parameters of regression lines is presented in Table 3. The best fit was obtained for Eq. (4) showing the lowest χ^2 value. The zero-porosity modulus value ($E_o = 327$ GPa) is also in very good agreement with the Young's modulus for polycrystalline silicon nitride reported in

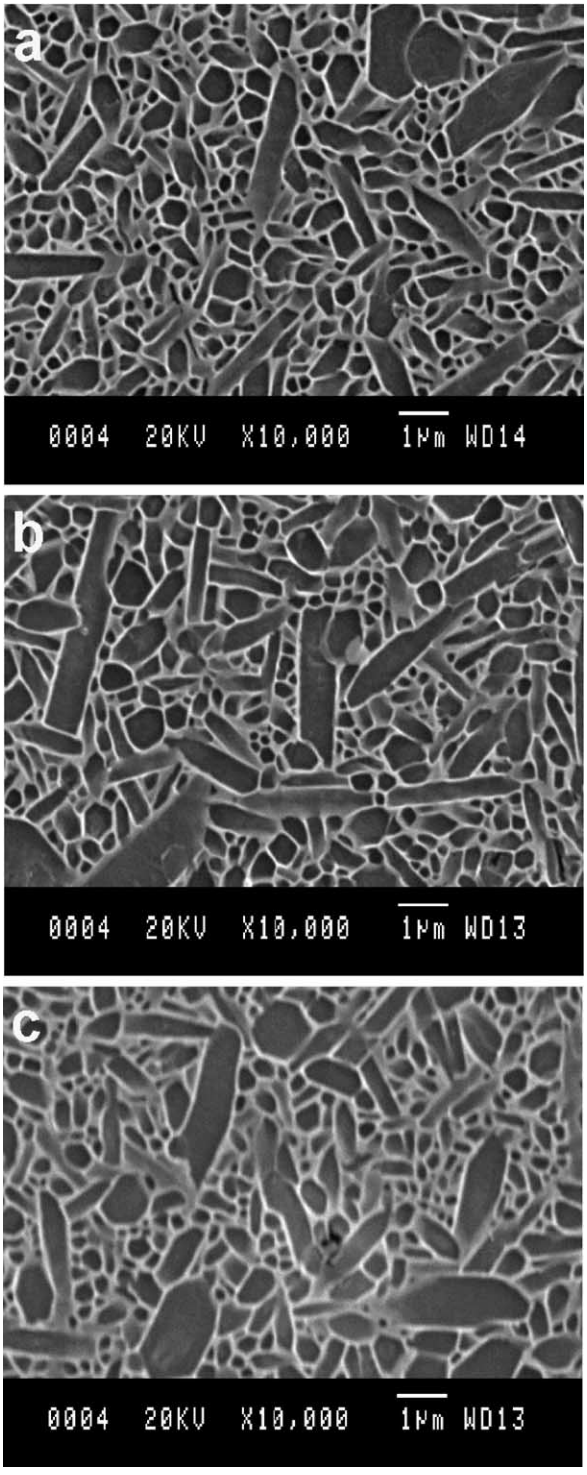

Fig. 4. SEM cross-section plasma etched micrographs of porous Si_3N_4 materials with (a) 0 vol.% starch, $P = 0.02$; (b) 10 vol.% starch, $P = 0.08$; (c) 20 vol.% starch, $P = 0.13$.

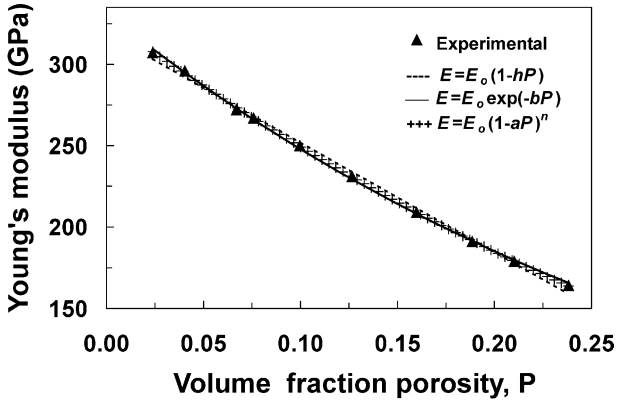

Fig. 5. Experimental values of the variation of Young's modulus as a function of volume fraction porosity, P, along with regression lines calculated for Eqs. (2)–(4).

Table 3
Summary of parameters of regression lines

Equation	E_o	Other parameters	χ^2
$E = E_o(1 - hP)$	319	$h = 2.11$	10.69
$E = E_o \exp(-bP)$	332	$b = 2.92$	2.52
$E = E_o(1 - aP)^n$	327	$a = 1.00$	1.04
		$n = 2.56$	

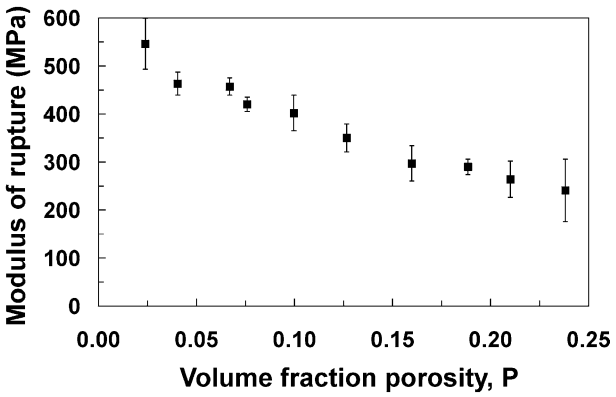

Fig. 6. Experimental values of the variation of modulus of rupture as a function of volume fraction porosity, *P*.

the literature, which typically fall in the range 300–330 GPa, depending on intergranular phase content, texture, relative amount of α and β phases and even residual porosity.[22] The *b* parameter in Eq. (3) can be correlated with pore geometry. The model of Rice[17] for spherical pores in cubic stacking arrangement predicts a value of 3, which is very close to the present work of 2.92 (Table 3).

The plots for the biaxial flexure strength expressed as modulus of rupture (MOR) measured as a function of porosity are shown in Fig. 6. The issue of applying minimum solid area or other models to the strength needs to be further addressed because of the fact that the pores may affect the flaw shape and especially the flaw size. A characterisation of other related properties, i.e. fracture toughness, in due course will be of much greater value in analysing mechanical performance–porosity behaviour of these materials.

4. Conclusions

Porous silicon nitride has been fabricated using a fugitive additive, corn starch, and samples have been produced with volume fractions of porosity from ~0 to 0.25. Final porosity, P, was controlled as a function of the starch content.

The microstructure consists of a dense matrix of elongated β-Si_3N_4 grains surrounded by intergranular glass phase and containing large pores and cavities. The average grain size was 0.26 μm and the mean aspect ratio was 3.7 and this did not vary with porosity.

The best fit for the Young's modulus–porosity relationship was obtained for the equation of the form: $E = E_o(1-aP)^n$. This dependency is also close to that for the MSA model for spherical pores in cubic stacking arrangement. The zero-porosity modulus values (E_o = 327–332 GPa) are also in very good agreement with those for silicon nitride reported in the literature, typically 300–330 GPa.

Acknowledgements

This work was supported by the Synergy Ceramics Project, NEDO, Japan, under an entrustment contract from the Fine Ceramics Research Association, Tokyo. Dr. Elis Carlström of the Swedish Ceramic Institute is gratefully acknowledged for helpful advice on processing of porous ceramics from starch. The authors wish to thank Dr. Bill Clegg of the University of Cambridge for use of plasma etching facilities and for useful discussions and Dr. Zoe Barber for assistance provided in the plasma etching of silicon nitride materials used in this work.

References

1. Jack, K. H., Review: Sialons and related nitrogen ceramics. *J. Mater. Sci.*, 1976, **11**, 1135–1158.
2. Riley, F. L., Silicon nitride and related materials. *J. Am. Ceram. Soc.*, 2000, **83**(2), 245–265.
3. Kawai, C. and Yamakawa, A., Effect of porosity and microstructure on the strength of Si_3N_4: designed microstructure for high strength, high thermal shock resistance, and facile machining. *J. Am. Ceram. Soc.*, 1997, **80**(10), 2705–2708.
4. Inagaki, Y., Tatsuki, O., Kanzaki, S. and Shigegaki, Y., Fracture energy of an aligned porous silicon nitride. *J. Am. Ceram. Soc.*, 2000, **83**(7), 1807–1809.
5. Yang, J. F., Ohji, T., Kanzaki, S., Díaz, A. and Hampshire, S., Microstructure and mechanical properties of silicon nitride ceramics with controlled porosity. *J. Am. Ceram. Soc.*, 2002, **85**(6), 1512–1516.
6. Kaskel, S. and Schlichte, K., Porous silicon nitride as a superbase catalyst. *J. Catal.*, 2001, **201**, 270–274.
7. Amaral, M., Lopes, M. A., Silva, R. F. and Santos, J. D., Densification route and mechanical properties of Si_3N_4–bioglass biocomposites. *Biomaterials*, 2002, **23**, 857–862.
8. Lyckfeldt, O. and Ferreira, J. M. F., Processing of porous ceramics by "starch consolidation". *J. Eur. Ceram. Soc.*, 1998, **18**, 131–140.
9. Blanks, K. S., Kristoffersson, A., Carlström, E. and Clegg, W. J., Crack deflection in ceramics laminates using porous interlayers. *J. Eur. Ceram. Soc.*, 1998, **18**, 1945–1951.
10. Slamovich, E. B. and Lange, F. F., Densification of large pores: I, experiments. *J. Am. Ceram. Soc.*, 1992, **75**(9), 2498–2508.
11. Davis, J. B., Kristoffersson, A., Carlström, E. and Clegg, W. J., Fabrication and crack deflection in ceramic laminates with porous interlayers. *J. Am. Ceram. Soc.*, 2000, **83**(10), 2369–2374.
12. Hampshire, S. Engineering properties of nitrides. In *Engineered Materials Handbook*. Vol. 4: Ceramics and Glasses, ed. ASM International, The Materials Information Society. ASM International, Materials Park, Ohio, 1992, pp. 812–820.
13. Kleebe, H.-J., Pezzotti, G. and Ziegler, G., Microstructure and fracture toughness of Si_3N_4 ceramics: combined roles of grain morphology and secondary phase chemistry. *J. Am. Ceram. Soc.*, 1999, **82**(7), 1857–1867.
14. Wötting, G., Kanka, B. and Ziegler, G., Microstructural development, mirostructural characterisation and relation to mechanical properties of dense silicon nitride. In *Proceedings of the International Conference Non-oxide Technical and Engineering Ceramics*, ed. S. Hampshire. Elsevier Applied Science, London, 1986, pp. 83–96.
15. Obenaus, P. and Herrmann, M., Method of Quantitatively characterising columnar crystals in silicon nitride ceramics. *Pract. Met.*, 1990, **27**, 503–513.

16. Dean, E. A. and Lopez, J. A., Empirical dependence of elastic moduli on porosity for ceramic materials. *J. Am. Ceram. Soc.*, 1983, **66**(5), 366–370.
17. Rice, R. W., Evaluation and extension of physical property–porosity models based on minimum solid area. *J. Mater. Sci.*, 1996, **31**, 102–118.
18. Rice, R. W., *Porosity of Ceramics*. Marcel Dekker, New York, 1998.
19. Roberts, A. P. and Garboczi, E. J., Elastic properties of model porous ceramics. *J. Am. Ceram. Soc.*, 2000, **83**(12), 3041–3048.
20. Phani, K. K. and Niyogi, S. K., Elastic modulus–porosity relationships in polycrystalline rare-earth oxides. *J. Am. Ceram. Soc.*, 1987, **70**(12), 362–366.
21. Phani, K. K. and Niyogi, S. K., Elastic modulus–porosity relationship for Si_3N_4. *J. Mater. Sci. Lett.*, 1987, **6**, 511–515.
22. Hay, J. C., Sun, E. Y., Pharr, G. M., Becher, P. F. and Alexander, K. B., Elastic anisotropy of β-Silicon nitride whiskers. *J. Am. Ceram. Soc.*, 1998, **81**(10), 2661–2669.